Wiley Analytical Science

Virtual Conference

The 5th edition of the Wiley Analytical Science Conference starts November 8, 2022!

Featured Session:

Weigh it right the first time in Karl Fischer titration

Tues Nov 15, 10:00 - 11:00 AM EST / 4:00 - 5:00 PM CET

events.bizzabo.com/WASconferenceFall2022

SARTORIUS

WILEY

Received: 10 May 2022 | Revised: 9 July 2022 | Accepted: 14 July 2022

DOI: 10.1002/app.52955

RESEARCH ARTICLE

Applied Polymer SCIENCE WILEY

Microfluidic-assisted preparation of nano and microscale chitosan based 3D composite materials: Comparison with conventional methods

Ceren Kimna | **Sibel Deger** | **Sedef Tamburaci** | **Funda Tihminlioglu**

Department of Chemical Engineering, İzmir Institute of Technology, İzmir, Turkey

Correspondence
Funda Tihminlioglu, Department of Chemical Engineering, İzmir Institute of Technology, Izmir, Turkey.
Email: fundatihminlioglu@iyte.edu.tr

Funding information
TUBITAK, Grant/Award Number: 116M096

Abstract

Although nanofillers contribute to improved physical characteristics and biological functionalities of polymer-based biomaterials, their dispersion in polymer matrices is still a challenging issue in terms of obtaining consistency for the inherent properties. To tackle this problem, homogenization techniques are applied to disperse the nanofillers in such polymers, however, these methods can cause undesired changes especially in the rheological properties and the physical structure of the biopolymer matrices. Recently, as a novel homogenization technique, microfluidization has been used to homogenize polymer nanocomposites to minimize these limitations. In this study, two different nanocomposite structures as chitosan/montmorillonite (CS/MMT) and chitosan/polyhedral oligomeric silsesquioxane nanocages (CS/POSS) were homogenized with microfluidization and investigated in terms of physical alterations. Furthermore, the effect of microfluidizer technique on material characteristics was compared with conventional homogenization techniques, i.e., ultrasonic bath and sonication in terms of solution, nano – (e.g., hydrodynamic size, drug encapsulation) and macroscopic material characteristics (e.g., porosity, mechanical properties, swelling and thermal degradation). It was found that the microfluidizer homogenization improves the physical characteristics in both nano and macroscale materials: Nanospheres obtained from CS/MMT composites showed enhanced stability, uniform size distribution (<100 nm, PDI: <0.2), and good encapsulation efficiency (>50%) whereas 3D porous CS/POSS scaffolds showed improved structural uniformity (i.e., homogeneous and interconnected microstructure) and enhanced thermal and mechanical properties. The obtained results indicate that the microfluidizer homogenization ensures a successful nanofiller dispersion in polymer matrices, thereby improving the biomaterial characteristics impressively compared to the sonication methods.

KEYWORDS
biomaterials, mechanical properties, microscopy, polysaccharides, porous materials

Ceren Kimna and Sedef Tamburaci have equal contribution in this study.

1 | INTRODUCTION

Biopolymers are widely preferred as fundamental material sources due to their various advantages in biomaterial fabrication. However, due to the comparably low stability of biopolymer-based materials, their structure is mostly reinforced with covalent (e.g., glutaraldehyde, carbodiimide) and transient crosslinkers (e.g., ionic and hydrophobic interactions).[1] As an alternative to crosslinkers, using nanoscale fillers as reinforcement agents is a great advantage in forming bio-nano composites by improving the physicochemical properties and the bioactivity of polymer matrices. It has been proven that nanofiller reinforcement shows promising developments in the functionality of the materials such as improved physicochemical properties,[2] enhanced biological properties such as better tissue regeneration,[3] osteoconductivity,[4,5] bioactivity,[6,7] and better control in drug delivery processes.[8–10] However, most of the nanoscale fillers tend to agglomerate and form clusters, and this non-uniformity in the nanoscale ends up in heterogeneity in material characteristics.[11] Several homogenization approaches such as ultrasonic method, mechanical shearing, or micro-scale techniques are applied to polymer-nanofiller dispersions to spread particles in the polymer matrix and obtain homogenous physical and chemical properties. In the ultrasonication process, the sound waves generate alternating high-pressure (compression) and low-pressure (rarefaction) cycles in the liquid phase. Sonication power, amplitude, time, and probe surface area are the parameters that describe the amount of energy delivered to the liquid phase and affect the particle dispersion in the suspension.[12] Ultrasonication is widely used for intercalation and distribution of nanofillers in biopolymer-based solution, however, it generally contaminates the solution by the erosion of metal ions on the sonicator probe. Conventional mechanical shearing can be an alternative, but the homogenization efficiency is relatively low compared to other methods. As an innovative technique, micro-scale methods can be promising alternatives to conventional methods with favorable properties such as easy processability and low energy consumption. Among these methods, microfluidization has come into prominence as a powerful technique for homogenization. Microfluidizer (MF) is a high-pressure homogenization technique that applies high shear stress to the solution in microchannels and can be evaluated as a bottom-up approach among the conventional composite formation techniques. The product enters the MF via the inlet reservoir and is forced to pass through microchannels by a high-pressure pump into the interaction chamber. A condenser pump inside provides the desired pressure to the product along the microchannels in the interaction chamber. The microfluidizer directs the product at constant pressure along the fixed geometry microchannel. The product is exposed to high-speed cutting rates in the interaction chamber. The velocity in microchannels can increase up to 500 m/s.[13] MF ensures that all the inlet material is homogeneously subjected to the same processing conditions. The effective process parameters of the microfluidizer process are pressure and the number of passes. The pressure and pass number induce homogenization and affect physiochemical characteristics.

MF homogenization has been used in various applications such as nano-emulsion and liposome production, high-pressure homogenization, breaking up particle clusters, and polymer degradation.[14–18] Recently, the use of microfluidizer homogenization to obtain uniform nanoparticles has gained increasing interest, especially in improving the encapsulation performance of carrier matrices.[19] For instance, Alkanawati et al.[20] compared the effect of microfluidizer homogenization and ultrasonication on the physicochemical properties of starch-based nanocarriers. By applying microfluidization, they not only achieve smaller nanoparticles but also obtain more uniform nanoparticle size distribution, possibly due to homogeneous energy provided compared to the energy produced by the cavitation-induced ultrasounds. Furthermore, Wei et al.[21] proved that microfluidizer homogenization prevents unwanted leakage of loaded agents (i.e., curcumin) from zein-propylene glycol alginate composite particles and increased particle stability. The physical and chemical properties of the polymers can be altered with MF operation. Therefore, the MF processing parameters (pressure and pass number) should be optimized to obtain a good dispersion level of particles in the polymer matrix to avoid degradation of the polymer structure, especially in biopolymers.

Literature findings indicate that homogenization techniques can drastically affect biopolymers' molecular weight due to the breakdown of covalent bonds in the macromolecule chain.[22–25] Up to now, a few studies have been conducted regarding MF as a homogenization technique for the nanocomposite formation.[13,26,27] Primarily, the effect of microfluidizer homogenization on the development of nanofiller-enriched biomaterials for biomedical applications has not been studied in detail. In this work, the microfluidization technique was used to homogenize polymer-nanoparticle solution to prepare chitosan-based nanocomposite biomaterials, which are commonly used biopolymers for various biomedical applications. In detail, two different chitosan-based nanocomposites were fabricated as nanospheres and 3D porous scaffolds with a combination of chitosan matrix with two different inorganic nanofillers. As a reinforcement agent, layered and cage-like nanoclays (i.e., sodium montmorillonite (MMT) and polyhedral oligomeric silsesquioxane nanocages (POSS),

respectively) were used to form chitosan-based composite materials. In detail, layered silicate MMT was dispersed in high molecular weight chitosan to form nanospheres for drug delivery whereas POSS, the smallest hybrid particles of silica, was incorporated into low molecular weight chitosan solution to form porous scaffolds. For these two nanocomposite materials, the effect of the microfluidizer treatment on nanofiller dispersion, polymer characteristics, and physical properties of the final biomaterials was investigated. Furthermore, the impact of microfluidizer treatment on 3D scaffold formation was compared with the conventional homogenization methods such as sonication and ultrasonic bath.

2 | MATERIALS AND METHODS

2.1 | Materials

High molecular weight chitosan (HMW CS; molecular weight: 310–375 kDa) and low molecular chitosan (LMW CS; molecular weight: 50–190 kDa) were obtained from Sigma-Aldrich (Schnelldorf, Germany). Organically modified montmorillonite (MMT, Cloisite 10A) was purchased from Southern Clay Products Inc (Gonzalez, TX). Gentamicin sulfate (Genta, IE Ulagay, Istanbul, Turkey) and vancomycin hydrochloride (Anko-L, Mustafa Nevzat, Istanbul, Turkey) were selected as model antibiotics for drug loading in nanospheres. POSS Octa TMA® (Hybrid Plastics, Hattiesburg, MS) was used for nanocomposite scaffold fabrication with LMW CS.

2.2 | Methods

2.2.1 | Preparation and characterization of CS/MMT and CS/POSS nanocomposite solutions

To obtain two different 3D structures with distinct morphologies, chitosan-based nanospheres and 3D microporous scaffolds were fabricated with high and low molecular weight chitosan, respectively. Briefly, the nanosphere-forming solution was prepared with 2% (w/w) HMW chitosan, which was solubilized in 90% (v/v) acetic acid solution and mixed overnight. MMT (3% w/w chitosan) was separately dispersed in distilled water (dH_2O) and mixed overnight to allow swelling. Next, clay dispersion was added to the chitosan solution dropwise. CS/MMT mixture was mixed for an additional 12 h and fed to the "Z" type interaction chamber of microfluidizer (Microfluidics®, LV1, Microfluidizer® Processors, USA) at 10000 and 20,000 psi pressure; cycled for 3, 5, and 10 passes for an efficient homogenization. The scaffold-forming solution was prepared with LMW chitosan, which was dissolved in 1% acetic acid solution with a concentration of 1% (w/w) of CS. Next, POSS nanoparticles were dried at 80°C under a vacuum for 24 h to prevent moisture and dispersed in dH_2O (10% w/w). Then, CS solution and POSS dispersion were gently mixed and fed to the microfluidizer to obtain a homogeneous LMW CS/POSS solution. Conventional homogenization methods, ultrasonic bath (ISOLAB, Eschau, Germany) and sonication with 15 and 35 Amplitude (Misonix Ultrasonic Liquid Processor, Farmingdale, NY) were also used in nanocomposite preparation for comparison. Both homogenization methods were applied for 30 min.

2.2.2 | Characterization of polymer solutions

Rheology

Polymer composite dispersions require a homogenization process for effective particle distribution in the polymer matrix. The high shear stress applied to biopolymers during the homogenization process can affect their rheological properties. Therefore, the effect of microfluidizer homogenization on the rheological properties of HMW chitosan was investigated using a rotational rheometer (Haake Mars II, Thermo Electron Corporation, Karlsruhe, Germany) in a cone/plate measuring system (with a 35 mm diameter and 2° angle). The shear stress (σ) was determined for shear rates ($\dot{\gamma}$) between 0 and 10 s^{-1}, and the average of five measurements was reported. To find the consistency index (K) and the flow behavior index (n) of the solutions, the power law was applied as follows:

$$\sigma = K\gamma^n \quad (1)$$

Viscosity and molecular weight determination

To determine the rheological behavior, intrinsic viscosities of HMW and LMW chitosan solutions were also examined with a capillary viscometer (SI Analytics, Typ513 10, App. Nr. 1067 23). Briefly, samples ($n = 3$) were fed to the capillary viscometer, and the flow time of the solvent and the solutions were recorded. Experiments were conducted at 25°C. The extrapolation of reduced viscosity determined the intrinsic viscosity to zero-concentration. Then, the viscosity-average molecular weight was calculated according to the Mark-Houwink-Sakurada equation below:

$$\eta = KM^{\alpha} \quad (2)$$

where K and α are constants specific to polymer, solvent, and temperature. The viscosity average molecular weight

was calculated from the equation where $K = 9.66 \times 10^{-5}$ (dm^3/g) and $\alpha = 0.742$ in the solvent system, composed of 0.15 M Ammonium acetate and 0.2 M Acetic acid solution at 25°C.[28]

Fourier transform infrared spectroscopy analysis

The effect of the microfluidizer homogenization on the deacetylation degree (DD %) of HMW and LMW chitosan matrices was determined using FT-IR analyses. The presence of nanofillers distributed in the polymer matrix was also detected with Fourier Transform Infrared Spectroscopy (FT-IR). First, solutions were pre-frozen at −20°C overnight and lyophilized for 48 h (Labconco-Freezone) at −46°C and under 0.01mBar vacuum. Before measurements, freeze-dried solutions were dehumidified under a vacuum at 35°C. Dried samples were analyzed with FT-IR (Shimadzu FTIR-8400S, Shanghai, China) by KBr pellet technique at wavelengths ranging from 4000 to 400 cm^{-1} and a resolution of 4 cm^{-1}. The peak heights were determined with IR Solution (Shimadzu) software. DD of the pure chitosan samples was calculated by the absorbance ratios of the amide-I band (at 1655 cm^{-1}) and OH^{-1} band (at 3450 cm^{-1}) using the equation derived by Domszy and Roberts (1985):[29]

$$DD\,[\%] = [1 - [(A_{1655}/A_{3450})\,/\,1.33]] \times 100 \qquad (3)$$

X-Ray diffraction

X-ray diffractograms of HMW chitosan. Na-MMT and CS/MMT dispersions were acquired in 2θ = 3–30° with a scan rate of 0.139°/second (Philips X'PertPro MRD). Before experiments, solutions were pre-frozen at −20°C overnight and lyophilized as described above. Diffraction patterns of the samples were analyzed at 40 kV using Cu-Kα radiation (λ = 1.54A).

2.2.3 | Fabrication and characterization of CS/MMT nanospheres

Chitosan/MMT nanospheres were fabricated by using the electrospraying technique. The nanocomposite solution was filled into a blunted syringe (21 G) and fed to the electrical field with a constant flow rate using a syringe pump. The operating conditions were adjusted as a voltage of 20 kV, 5 ml/h flow rate, and 10 cm distance between syringe and collector surface. Fabricated CS/MMT nanospheres were kept in a desiccator at RT for further characterizations in terms of morphology, particle size, and encapsulation efficiency, which are significantly affected by nanofiller distribution in a polymer matrix with homogenization process.

Effect of homogenization on morphology and particle size

SEM analysis. The morphology of the nanospheres was examined with Scanning Electron Microscopy (SEM, Quanta FEG 250, FEI Inc., USA). Before analysis, samples were coated with gold under an Argon atmosphere (Emitech K550X, Kent, UK). The diameter of nanospheres was measured as an average of a minimum of 250 individual spheres using the Image J software.

Dynamic light scattering analysis and determination of zeta potential. The nanospheres' hydrodynamic size and zeta potential were determined with light scattering using a Nano ZS zeta sizer (Malvern Instruments, Herrenberg, Germany) with a backscatter angle of 173°. Before measurements, samples ($n = 3$) were dispersed in distilled water and vortexed, and the mean hydrodynamic diameters were analyzed as intensity average distributions. The zeta potential of the nanospheres was investigated with Malvern Zetasizer Nano-Zs. Samples ($n = 3$) were analyzed in 1× PBS (pH = 7.4) and ultrapure water at 25°C. Samples were dispersed in liquid media, vortexed, and studied with 3 runs and 100 scans per run.

Effect of homogenization on drug encapsulation efficiency. Two model antibiotics, Gentamicin sulfate (GC) and Vancomycin hydrochloride (VC), were incorporated into the sphere-forming nanocomposite formulation to investigate the drug entrapment efficiency of nanospheres. To do so, GC and VC were dissolved in HMW chitosan solution before the MMT addition with a total polymer to drug ratio (P:D) of 20:1 and 8:1, respectively. The homogenization and electrospraying steps were applied to drug-incorporated solutions as described above. Obtained nanospheres were dispersed in 5 ml of PBS (pH = 7.4), disrupted in an ultrasonic bath for 30 min, and filtrated. The total amount of entrapped drug in the nanocomposite matrix was determined spectroscopically at 256 and 282 nm for GC and VC, respectively (Varioskan, Thermo Fisher Scientific, MA, USA). The encapsulation efficiency (EE) of the nanospheres was calculated as follows:

$$EE\,[\%] = \frac{amount\ of\ drug\ entrapped\ in\ nanospheres\,[mg]}{amount\ of\ initial\ drug\ feed\,[mg]} \times 100 \qquad (4)$$

2.2.4 | Fabrication and characterization of CS/POSS scaffolds

Porous LMW CS/POSS scaffolds were obtained with the freeze-drying technique. Briefly, the solutions were

homogenized with different techniques, then molded in 24-well plates, pre-frozen at −20°C overnight, and freeze-dried for 48 h at −46°C and under 0.01 mbar vacuum. Fabricated scaffolds were kept in a desiccator at RT until further characterization tests in terms of morphology, mechanical characteristics, and swelling properties.

Effect of homogenization on morphological characteristics

SEM and micro CT analyses. The homogenization process, which affects the viscosity of polymer composite solution, may lead to alterations in 3D structure and porosity. Therefore, scaffold structure was determined with SEM to investigate the effect of the homogenization process on morphology and 3D microstructure as well as average pore size and porosity. Samples were first prepared for the SEM analysis as described above, and the lateral pore sizes were determined using Image J software by the obtained SEM micrographs. 3D morphology and structure of the scaffolds were also analyzed using a computerized microtomography method (Scanco-μCT50, Scanco Medicals, Switzerland) with the real resolution at 45 kVp and 88 uA. Scaffolds were scanned through 500 slices with a 3 μm voxel size in micro-Ct analyses. Average pore size, total porosity, and interconnections of porous structures were determined with micro-CT analyses.

Liquid displacement method. The liquid displacement method was used to calculate the percentages of open pores in the scaffold. For this study, scaffold samples ($n = 3$) were placed into a measuring cylinder containing 20 ml of 100% ethanol (V_1) and placed in a vacuum oven to replace the entrapped air in the open pores with ethanol. Next, the volume overflowing with the scaffold (V_2) and the decreasing volume (V_3) after the scaffolds were recorded. The open porosity (%) was measured with the equation given below:

$$\epsilon = (V_1 - V_3)/(V_2 - V_3) \quad (5)$$

Effect of homogenization on physical properties

Mechanical properties. Mechanical properties of fabricated scaffolds were determined with the compression test using TA XT Plus Texture Analyzer (Stable Micro Systems, UK). Experiments were conducted according to the ASTM D-5024 standard. A 5 kgf load cell was used at a testing speed of 3 mm/min.

Water absorption capacity. Swelling tests were performed to determine the water absorption capacity of the scaffolds. Prior to tests, samples were neutralized with a 1 M NaOH solution for 30 min. Then, scaffolds were immersed in 1x PBS (pH = 7.4) at 37°C for 48 h. The swelling ratio of scaffolds (SR) was determined according to the relation between the weight of wet (W_w) and dry samples (W_d):

$$SR = (W_w - W_d)/W_d \quad (6)$$

Thermal gravimetric analysis

The thermal stability of LMW CS and CS/POSS composites was assessed via thermogravimetric analysis to investigate the effect of different homogenization techniques on chitosan matrix (Perkin Elmer Diomand TG/DTA). Analyses were performed under a nitrogen atmosphere in the temperature range of 30–650°C at a heating rate of 10°C/min.

3 | RESULTS AND DISCUSSION

In this study, the microfluidization technique was used to homogeneously disperse two different nanofillers in a biopolymer matrix for different biomedical aspects. As a base matrix material, natural biopolymer chitosan was selected due to its good biocompatibility,[6,30] antimicrobial activity,[31,32] and biodegradability,[33] which makes it one of the ideal polymer materials for biomedical applications.[34] Therefore, high- and low-molecular-weight chitosan was used to prepare nanocomposites with two fillers, that is, MMT and POSS, respectively. Homogeneous dispersion of these nanofillers is a challenging issue due to the agglomeration tendency of nanoparticles in the polymer solution. Thus, homogenization techniques were generally used for the preparation of nanocomposite solutions. This is the point at which microfluidization is an efficient and novel homogenization technique to overcome the possible non-uniformity in the polymer matrix. However, the homogenization process leads to changes in the physical properties of polymer solutions that eventually affect the physical characteristics and lead to changes in morphology and characteristics of the fabricated polymer matrix. From this point of view, chitosan solutions were investigated regarding rheological behavior and viscosity. Then fabricated nanocomposites were investigated in their physical and morphological characteristics to observe the effects of the homogenization process on material characteristics.

3.1 | Rheological behavior

Microfluidizer treatment applies high pressure to the polymeric solutions in microchannels to homogenously

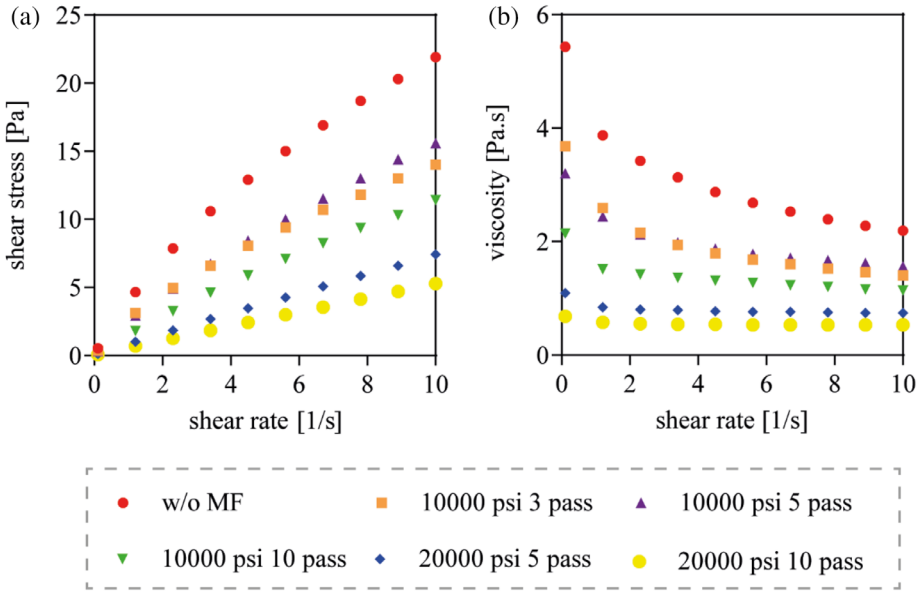

FIGURE 1 Flow curve (a) and viscosity curve (b) of HMW chitosan treated with different microfluidizer parameters [Color figure can be viewed at wileyonlinelibrary.com]

distribute nanofillers/nanoparticles in a polymer matrix. However, the working parameters should be well-optimized for the applications, especially with the natural polymers, since factors such as high pressure and temperature increase with the cyclic application might cause an irreversible change in the polymer characteristics. Therefore, the effect of microfluidizer pressure and pass number on rheological properties of HMW chitosan solution was investigated with a rotational rheometer equipped with a cone/plate geometry. LMW CS solutions, however, could not be analyzed with this set of equipment due to their highly aqueous structure and low viscosity. Figure 1 represents the shear-dependent stress (a) and viscosity (b) of MF-treated HMW chitosan solutions, respectively. It was observed that the viscosity of HMW-CS samples decreased with the increment of the shear rate (Figure 1b). This shear-thinning (or pseudo-plastic) behavior is generally found in polymeric solutions. The experimental viscosity versus shear rate fit the power-law well with high regression coefficients ($R^2 > 0.99$). The rheological parameters, together with the apparent viscosity and shear stress values, were shown in Table S1 in the supplementary file. Apparent viscosities were calculated at the shear rate of 10 s^{-1}. As usual for shear-thinning fluids, the flow behavior index n is smaller than 1.[35] Results implied that MF caused a change in rheological properties of HMW chitosan solution, especially in high pressure and pass numbers. Groups with a pass number of 3 and 5 at constant pressure (10,000 psi) showed similar rheological properties. Increasing the pressure from 10,000 to 20,000 psi, however, significantly affected the solution characteristics, and the viscosity of the solution changed from shear-thinning to almost Newtonian behavior. It was found that the pressure had more impact on the solution viscosity than the pass number. The decrease in viscosity can be attributed to polymer chain degradation, conformational change, and a decrease in molecular weight. Literature findings also indicate that the apparent viscosity of the chitosan solution containing lemongrass essential oil has been significantly reduced with a high-pressure homogenization.[16]

3.2 | Molecular weight determination

A change in the biopolymer's molecular weight significantly affects the fabricated material's physicochemical characteristics, leading to tremendous changes in its functionality and bioactivity. It has been shown that MF homogenization affects the physical properties of biopolymer-based materials due to the application of high pressure through the microchannels.[36–38] Therefore, to be able to assess these possible responses, first, the molecular weight of high- and low molecular weight chitosan solutions was determined with a capillary viscometer. Here, the viscosity-average MW of the solutions was further used to calculate the intrinsic viscosity and the molecular weight through the equation Mark-Houwink-Sakurada empirical correlation. However, the HMW CS groups homogenized with 20,000 psi were eliminated due to their very low viscosity, which is not desired for the nanosphere fabrication technique that we aim to use. As shown in Table S2, the MW of solutions decreased with an increase in the pressure and pass number due to the inflated energy flow that leads to polymer degradation. However, the MF treatment caused a very slight change in the molecular weight at 10000 psi and 3 passes for HMW and 5000 psi with 3 passes for LMW, respectively.

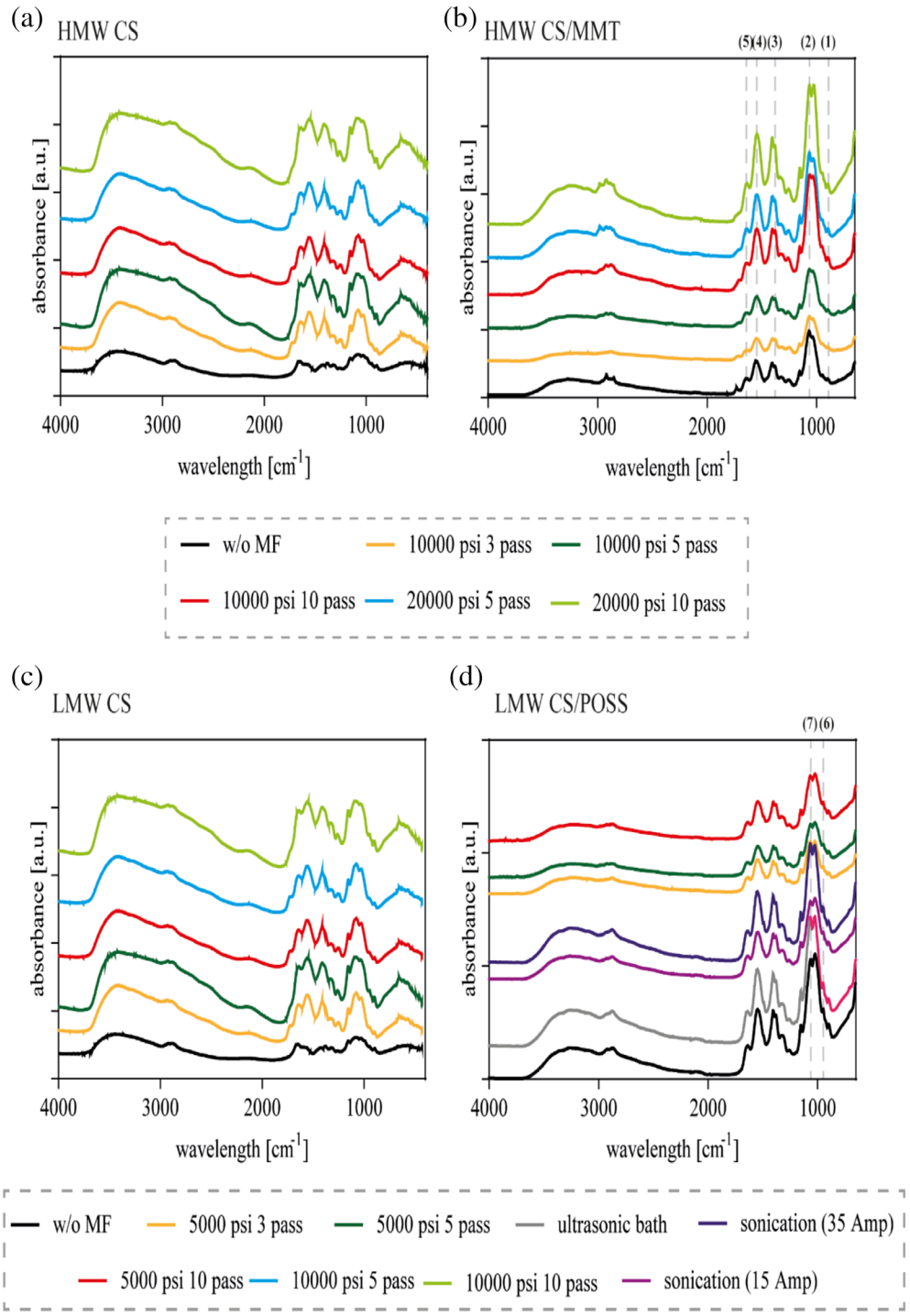

FIGURE 2 FT-IR spectra of HMW CS (a), HMW CS/MMT composite (b), LMW CS (c), and LMW CS/POSS composite (d) treated with different homogenization parameters [Color figure can be viewed at wileyonlinelibrary.com]

After that point, it was observed that the molecular weight sharply decreased. At 10000 psi, the molecular weight of HMW chitosan decreased from 131.0 to 101.4 kDa when the pass numbers increased from 3 to 5 passes. The MW was further reduced to 68.55 kDa with MF conditions at 10000 psi with 10 passes, which can be attributed to reduction due to chain scission of chitosan backbone.

Similarly, the molecular weight of LMW chitosan decreased from ~98.8 to 45.1 kDa at 5000 psi and 5 passes of MF application. To compare the effect of a microfluidizer with an alternative homogenization method, high molecular weight chitosan solution was treated with a sonicator probe for 30 min. Results indicated that intrinsic viscosity decreased drastically and molecular weight as 169, and 23.5 kDa, respectively (Table S2). Although a similar homogenization technique was applied to LMW chitosan, ultrasonic bath homogenization did not affect the molecular weight and caused a slight molecular weight decrease from 98 to 91 kDa. On the contrary,

TABLE 1 Deacetylation degree of HMW and LMW chitosan treated with different microfluidizer parameters

Polymer	MF parameters	Deacetylation degree (%)
HMW CS	Non homogenized	77.5 ± 2
	10,000 psi 3 passes	80.9 ± 2
	10,000 psi 5 passes	80.9 ± 2
	10,000 psi 10 passes	84.3 ± 1
	20,000 psi 5 passes	80.3 ± 1
	20,000 psi 10 passes	84.9 ± 3
LMW CS	Non homogenized	75.1 ± 0
	5000 psi 3 passes	75.2 ± 0
	5000 psi 5 passes	77.9 ± 0
	10,000 psi 3 passes	71.3 ± 0
	10,000 psi 5 passes	75.2 ± 0

ultrasonicated LMW chitosan exhibited a remarkably reduced molecular weight of 30 and 33 kDa with sonication amplitudes at 15 and 35, respectively.

3.3 | FT-IR and XRD analyses

The deacetylation degree of chitosan treated with different homogenization conditions was evaluated with FT-IR analyses. The relation regarding the absorbances of the bands at 1655 cm^{-1} (the amide I band, which represents the residual —CO—NH— groups) and at 3455 cm^{-1} (OH bar, which is used as a reference band) was used to calculate the DD. First, the characteristic peaks of chitosan spectra at amide III (1380 cm^{-1}, Figure 2b, line 3), amine (1560 cm^{-1}, Figure 2b, line 4), and amide I (1655 cm^{-1}, Figure 2b, line 5) peaks were determined for two chitosan composite groups. When the amide band at 1655 cm^{-1} for pure chitosan spectra was evaluated, a decay at different treatment conditions was observed due to the possible transformation of acetamide groups into primary amine groups, thus, leading to an increase in the DD (Figure 2a, c). The deacetylation degrees of the chitosan solutions at different MF conditions were given in Table 1. The DD of the HMW chitosan without MF was calculated as ~77.6%, which was found reasonable since the original product was described as >75% deacetylated. However, the MF-treated samples showed a higher DD (80–85%) compared to the non-treated sample. Results indicated that the pass number affects the deacetylation degree more when compared to the effect of pressure. On the contrary, it was observed that this homogenization step did not cause a significant change in the deacetylation degree of LMW chitosan. Additionally, these findings fit well with previous studies regarding the microfluidizer treatment of chitosan for other applications.[22] The deacetylation of chitin results in the formation of free amine groups that gives the solubility property to chitosan, so it is one of the most important physicochemical parameters that affect the physical, chemical, and biological properties of the chitosan-based materials.[39,40] Together with the visual observations of the solutions, such a harmful effect, i.e., lowered solubility, was not observed for both high and low molecular weight chitosan. FT-IR analysis was further performed to determine the presence of nanofillers in HMW CS/MMT and LMW CS/POSS composites (Figure 2b, d) or any interactions between CS and fillers. The representative peaks of MMT were determined at the groups at 913 cm^{-1} (Figure 2b, line 1) due to Al-Al-OH, and an explicitly sharp peak at 1070 cm^{-1} (Figure 2b, line 2) representing Si—O—Si stretching,[41] which confirms the presence of nanoclay in the chitosan matrix. Upon subjecting CS/MMT samples to the microfluidizer homogenization, the characteristic peaks of chitosan at 1655 cm^{-1} (amide I bonds), 1560 cm^{-1} (amine bonds), and 1380 cm^{-1} (amide III bonds) slightly shifted to left in CS/MMT composite. Furthermore, the N–H stretching band (3295 cm^{-1} – 3370 cm^{-1}) became broader with the microfluidizer application. When the pass number was increased, it was observed that the pattern at 1560 cm^{-1} indicating the N–H bending of chitosan was slightly shifted to 1570 cm^{-1}, which can be possibly explained by the favorable interactions between the entrapped water in MMT layers and the N–H of chitosan.[42]

Similarly, the presence of POSS nanoparticles in the chitosan matrix was proven with FT-IR analysis. Here, the FTIR spectrum of composites homogenized with other methods, i.e., ultrasonic bath and sonication, were also tested and compared. In all LMW CS/POSS groups, a strong Si—O—Si stretching absorption band at 1070 cm^{-1} (Figure 2d, line 7) was obtained. Additionally, a slight peak observed at 920 cm^{-1} (Figure 2d, line 6) was attributed to the torsional vibration of NMe4 groups that exhibits in the POSS structure.[43] Furthermore, a peak at 1680 cm^{-1} was observed at all the samples treated with microfluidizer homogenization, which is a signature peak of C═O stretching of the newly formed amide bond in the composites.[44] These characteristic peaks of POSS nanocage in the FT-IR spectra again approves that the nanoparticles were successfully incorporated into the matrix.

Diffraction patterns of HMW CS, Na-MMT, and CS/MMT solutions treated with microfluidizer homogenization (10,000 psi 3 and 5 passes) were characterized using XRD as depicted in Figure 3. The results show that non-processed CS samples showed the main chitosan peak in the 2θ range of 20–25°.[45] However, after

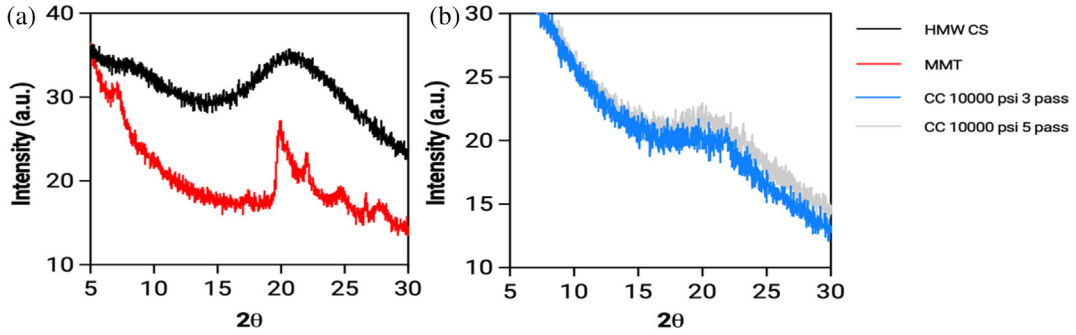

FIGURE 3 XRD diffractograms of (a) HMW chitosan, Na-MMT and (b) CS/MMT composites that are homogenized with microfluidizer [Color figure can be viewed at wileyonlinelibrary.com]

microfluidizer treatment, the signature chitosan peak had a lower amplitude for both groups, which can be attributed to the increased disarray in chain alignment compared to the non-processed, pure chitosan samples (Figure 3b). <001> diffraction of Cloisite 10A nanoclay indicated 2θ values of 4.65 (Figure 3a), however, the disappearance of <001> reflection of Cloisite 10A nanoclay in the MF processed CS/MMT composites can be attributed to exfoliation of layered silicates in the CS matrix (Figure 3b) that indicates the good dispersion of MMT with MF homogenization in CS matrix.

3.4 | The effect of homogenization on CS/MMT nanospheres

So far, the experiments were conducted with the solubilized or freeze-dried samples to show the effect of the homogenization step on the material-forming solutions. In the next step, the HMW CS/MMT nanocomposite solution was electrosprayed to form nanospheres under predetermined conditions. SEM images indicated that, both HMW CS and HMW CS/MMT nanocomposite processed with different microfluidizer parameters were able to form spherically shaped, dry nanospheres whereas, non-uniform nanosphere-fiber forms were obtained with conventional homogenization methods (ultrasonic bath, sonication with 15–35 Amp) (Figure 4). These homogenization methods caused unfavorable conditions for the electrospray process due to the significant decrease in CS/MMT solution viscosity. However, observations showed that the pressure increase impeded dry nanospheres' formation under these conditions. Therefore, groups homogenized at 20000 psi pressure could not be further used to characterize nanospheres. This effect could be explained by the low viscosity of this group that negatively affected the continuous jet conditions in electrospray, which requires either increasing the distance between the collector and the syringe needle or the nanofiller amount in the nanocomposite.

On the other hand, nanocomposite groups homogenized with a microfluidizer at 10000 psi pressure could be used to form spherical, uniform nanoparticles with a dry size range of 31–76 nm (Table 2). Histogram data in Figure 4 also indicated that MF homogenization decreased the nanosphere size range compared to the non-homogenized CS group. Besides, an increase in pass number induced this size change by reducing the diameter range from 50–500 to 20–200 nm with a 10 pass number.

Light scattering measurements were performed to investigate the hydrodynamic sizes of nanoparticles and the homogeneity of chitosan matrix. MMT nanofiller ensured the stability by acting as a physical cross-linker for CS/MMT nanospheres homogenized with MF at 10000 psi. In literature, it was indicated that the MF treatment induces the conformational changes in the polymer chain and the number of charged groups is increased in the polymer hydration surface.[22] Therefore, it is likely that the cyclic application of MF caused improved interactions between cationic chitosan and negatively charged MMT interlayers. The intensity average hydrodynamic size distributions of CS/MMT nanospheres were depicted in Table 2. The group treated with 10,000 psi and 5 passes resulted in the smallest average size (65 ± 4 nm) with a very low polydispersity index (PDI, 0.10), which confirms the visual observations as obtained by the SEM imaging. Zeta potential of the CS and CS/MMT nanospheres was investigated at pH = 7.4. The zeta potential of the unmodified chitosan without a nanofiller reinforcement was found to be highly positive (24.0 ± 3.6 mV) due to the protonation of the primary amine groups of chitosan. The zeta potential of the nanocomposite spheres was also found in the positive range, which shows that the chitosan dominated the overall surface charge. MMT incorporation resulted in comparably lower zeta potential values (6–14 mV) due to the net negative charge of surface silicate layers of MMT platelets in the working pH. However, it was observed that with the

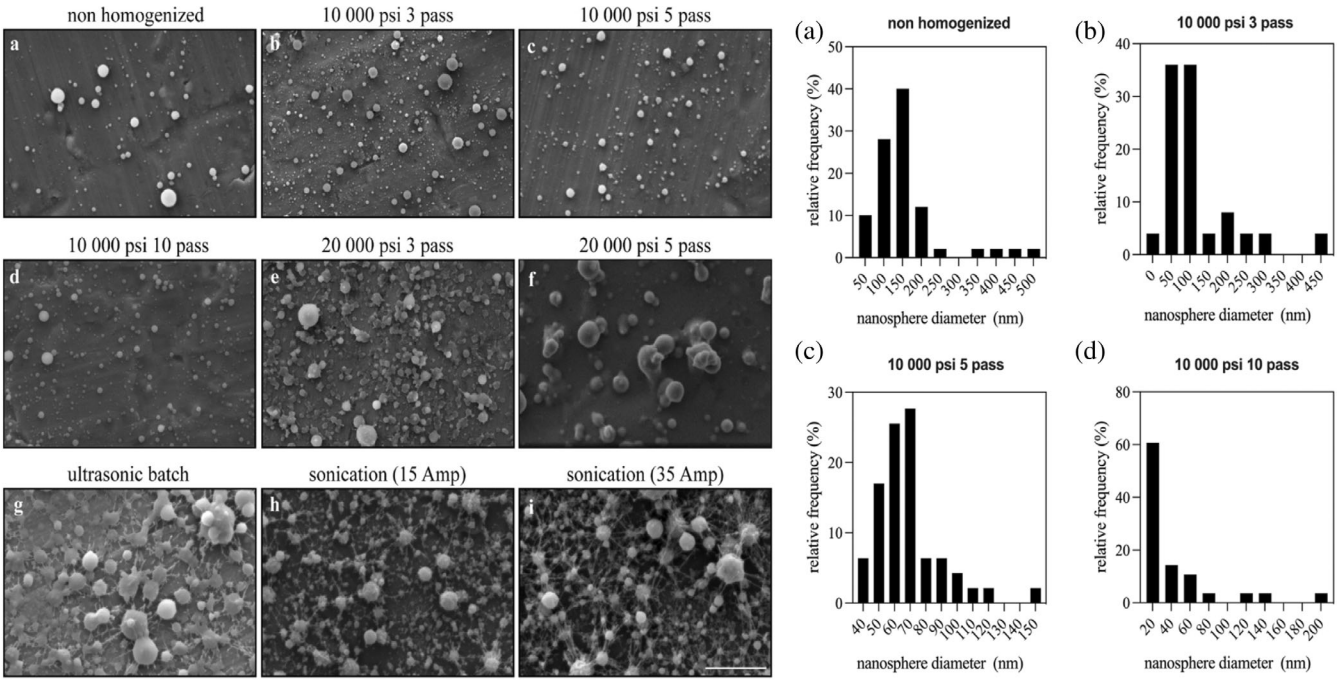

FIGURE 4 SEM images of electrosprayed, non-homogenized HMW CS (a) and HMW CS/MMT nanospheres treated with different MF conditions (b-f), ultrasonic batch (g), and sonicator (h, i). Images were acquired with an accelerating voltage of 5 kV; scale bar represents 2 μm

TABLE 2 Average size, hydrodynamic size, polydispersity index (PDI), and the zeta potential of CS/MMT nanospheres

MF parameters	Average size SEM (nm)	Average hydrodynamic size DLS (nm)	PDI	Zeta potential (mV)
Non homogenized	117 ± 34	166 ± 41	0.86	24.0 ± 3.6
10,000 psi 3 passes	77 ± 27	207 ± 30	0.53	6.40 ± 1.0
10,000 psi 5 passes	59 ± 14	65 ± 4	0.10	13.3 ± 1.3
10,000 psi 10 passes	31 ± 12	15 ± 5	0.40	13.7 ± 7.5

increase from 3 to 5 pass, the net negative surface charge of the nanospheres was increased from 6 to 13 mV due to possible improvement in the dispersion of the platelets in the chitosan matrix. This remarkable difference was not observed with the increase in the pass number to 10. However, the average hydrodynamic size was reduced. The positive zeta potential of CS/MMT nanospheres was found to be beneficial for further use in many delivery strategies such as intracellular delivery and mucoadhesive systems.[46,47]

As indicated before, the deacetylation degree plays an important role in the crosslinking and stability of chitosan-based systems, which are the essential factors, especially for the nanoscale drug delivery systems. In the study of Gupta and Jabrail (2006), it has been shown that the increase in the deacetylation degree of chitosan causes higher encapsulation efficiency, and consecutively a higher control over the release rate for chitosan-based microspheres.[48] Therefore, such effects of the deacetylation degree and the improved nanofiller dispersion on drug carrier nanospheres were evaluated. Here, two different antibiotics (GS and VC) were used as model drugs, and the polymer to drug ratio was adjusted for each formulation regarding the solubility of the antibiotics. Again, a determination of the encapsulation efficiency was not possible for the unmodified control CS nanospheres due to the aforementioned stability problem. The VC EE % of CS/MMT nanospheres varied between 55% and 85%, whereas GC EE % was in the range of 64–95% (Table 3). For both drugs, interestingly, a similar effect was observed in EE by changing homogenization parameters: The EE of the nanospheres homogenized with 3 passes was found to be lowest and remarkably increased with the application of 5 passes due to a possible improvement in the dispersion of the nanoclay sheets in the biopolymer matrix.

Furthermore, EE of the nanospheres decreased when the pass number was increased to 10. This could be

TABLE 3 The encapsulation efficiency of nanospheres treated with different MF parameters

MF parameters	VC encapsulation efficiency (%)	GC encapsulation efficiency (%)
10,000 psi 3 passes	56 ± 19	72 ± 24
10,000 psi 5 passes	86 ± 2	93 ± 6
10,000 psi 10 passes	72 ± 36	64 ± 19

explained by the homogeneity and yield of the nanoparticles under these working conditions. By considering the results together with the observations and the nanosphere-forming solution properties such as increased deacetylation degree, one can conclude that the CS/MMT nanospheres showed remarkably improved characteristics with the good homogenization of the MMT nanofillers.

3.5 | The effect of homogenization on CS and CS/POSS nanocomposite scaffolds

3.5.1 | Morphology and 3D structure

LMW CS/POSS nanocomposite dispersion was used for the fabrication of 3D microporous scaffolds. POSS nanoparticles were utilized as nanofiller reinforcement to obtain a nanocomposite structure for hard tissue regeneration. However, biomaterials should meet several criteria to be considered as a biomaterial, for example, adequate pore size and morphology, good mechanical properties, biodegradability, and biocompatibility. Since the biocompatibility of the chitosan-based materials was successfully proven in various applications,[49,50] in this study, the effect of the homogenization parameters on macro-and microstructure and the physical properties of the scaffolds were focused on in detail. First, SEM analysis was performed to determine the morphology, microstructure, and average lateral pore size of the CS and CS/POSS scaffolds.

The effect of ultrasonic bath, sonication, and microfluidizer conditions on porous structure and the pore walls of scaffolds was determined (Figures 5- 8), and the average lateral pore sizes were calculated with Image J software and given in Table 4. Conventional homogenization techniques such as ultrasonic bath and sonication did not significantly alter the average pore size of CS scaffolds compared to non-homogenized CS. Histograms showed similar pore size distribution for non-homogenized CS; ultrasonic bath homogenized CS and CS group sonicated at 15 amplitudes. However, increasing the amplitude of sonication from 15 to 35 led to an increase in the pore size by altering the pore structure and changing the pore size distribution range (159–267 μm) (Figure 5). In addition, the sonication technique changed the pore walls into thinner interconnected structures due to their decrease in molecular weight and viscosity. It was observed that the microfluidizer homogenization with 5000 psi and 3 passes caused cracks on the pore walls and caused the formation of a non-homogeneous structure. However, when the pass number is increased to 5, homogenous pore morphology and microstructure were achieved (Figure 6). Histograms of CS/POSS scaffolds indicated that ultrasonic bath and sonication at 15 amplitudes enhanced the pore size compared to pure CS scaffolds (Figure 7). However, the pore size distribution range decreased as the pressure and pass number increased in microfluidizer homogenization (Figure 8). This led to homogeneity in pore size and morphology. However, microstructure deteriorations and elongation of the pore walls have occurred in LMW CS/POSS composite scaffolds with microfluidizer homogenization, unlike pure LMW CS scaffolds. With increased pressure (10,000 psi, 5 passes), the pore walls of CS/POSS scaffolds became thinner (Figure 8). SEM images showed that the MF-processed scaffolds obtained by lyophilization could mimic the porous structure of the trabecular bone. The literature reported that the pore sizes in a range of 75–250 μm had optimum pore diameter in bone scaffolds.[51] Also, it was found that the macropores larger than 100 μm were suitable for cell migration, vascularization, and bone tissue formation, and these sizes ensure cell migration and transport.[52]

Larger pores in the range of 100–150 and 150–200 μm are required for substantial bone in-growth, whereas pores in the range of 75–100 μm provide an appropriate microenvironment for unmineralized osteoid tissue in-growth. Smaller pores (10–44 and 44–75 μm) are penetrated only by the fibrous tissue.[53] Here, the average pore size of CS and CS/POSS scaffolds were found in the appropriate range (199–283 μm) (Table 4). In addition to that, it is known that an ideal scaffold should have open pores that could provide successful nutrient and gas transfer. Therefore, the open pore percentage of CS/POSS scaffolds was determined with the liquid displacement method as 70–85% (Table 4). These values were, again, found to be sufficient to mimic the trabecular bone tissue with a 50–90% porosity.[54] Among the dispersions homogenized with the microfluidizer, the highest open porosity was obtained in the groups with the working conditions of 10,000 and 5000 psi with 3 cyclic passes. According to the observations, a further increase in the pass number caused the formation of less porous structures due to the change in polymer solution viscosity.

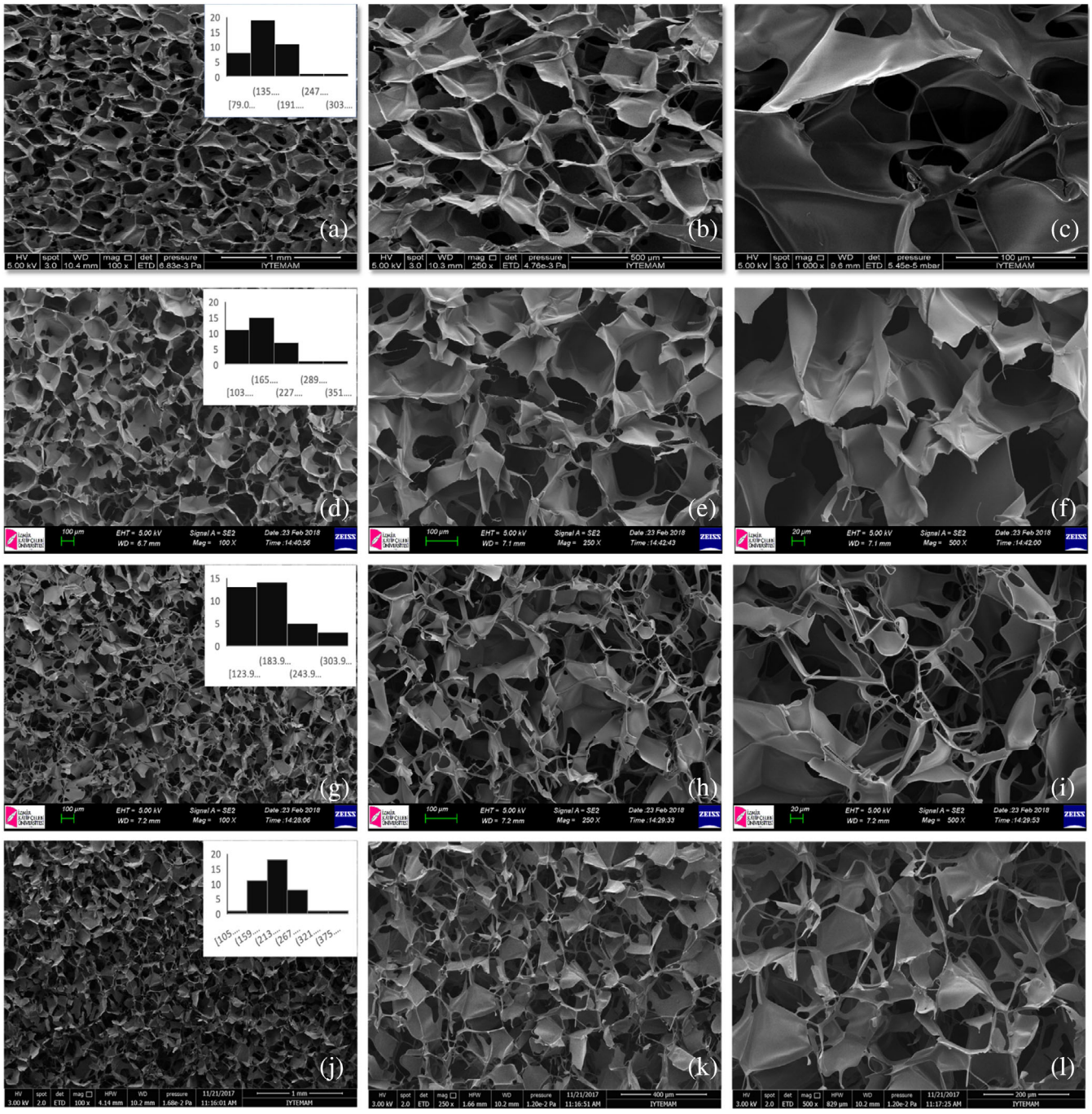

FIGURE 5 SEM images of non-homogenized LMW CS (a, b, c) and LMW CS scaffolds treated with ultrasonic bath (d, e, f); sonicator-15 amp (g, h, i); sonicator-35 amp (j, k, l) in magnification of 100×, 250×, and 500× [Color figure can be viewed at wileyonlinelibrary.com]

3D structure of the CS and CS/POSS scaffolds was also evaluated with micro-CT analysis (Figures 9 and 10). Scaffolds showed highly interconnected, porous microstructures with a porosity varying between 87.5 and 89.8% (Table 4). Nonhomogenized CS scaffolds showed layered structures in the peripheral parts and more compact pore morphology in the interior. Moreover, weak and non-uniform interconnections were observed (Figure 9a). Cross-sectional images indicated that scaffolds treated with ultrasonic bath and sonication processes showed weak pore interconnections. In contrast, microfluidization induced highly interconnected pore structures (Figure 9b-f and Figure 10a-e). On the other hand, micro-CT images of the microfluidizer-treated scaffolds showed uniform and branched microstructures with interconnected open pores. Additionally, the cross-sectional slides taken from the middle part of the scaffolds showed that the homogenous interconnected

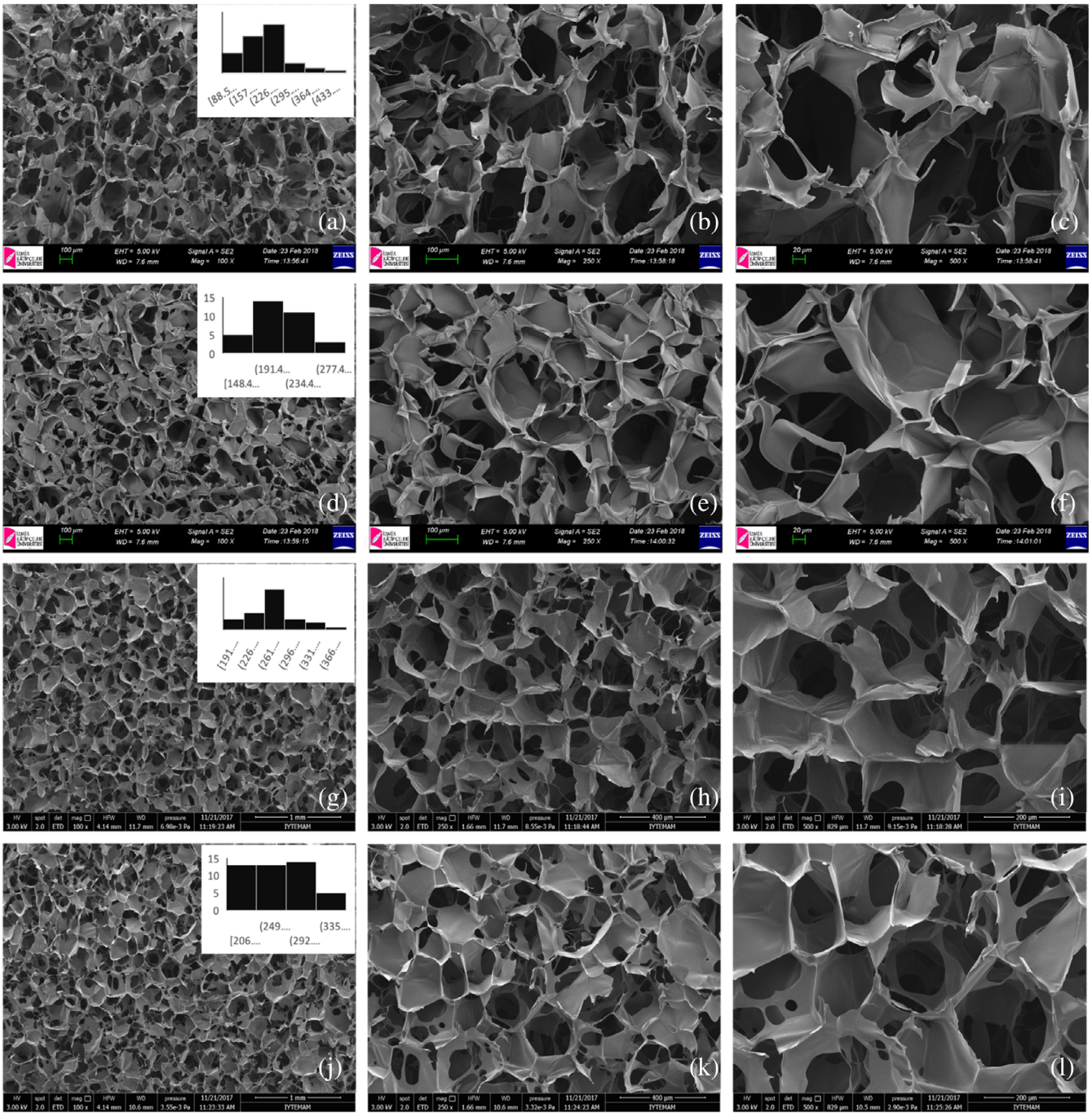

FIGURE 6 SEM images of LMW CS scaffolds treated with microfluidizer homogenization. Microfluidizer parameters are: 5000 psi 3 pass (a, b, c); 5000 psi 5 pass (d,e,f); 10,000 psi 3 pass (g, h,i); 10,000 psi 5 pass (j, k, l) in magnification of 100×, 250×, and 500× [Color figure can be viewed at wileyonlinelibrary.com]

structure did not change within the matrix. However, groups homogenized with ultrasonic bath and sonicator showed weak and shorter interconnections. The obtained microstructure herein is preferred in the scaffolds to be used as an implant material to deliver nutrient-liquid transport and allow for vascularization. Micro-CT results indicated that microfluidizer homogenization did not have a negative effect on the microstructure of scaffolds.

3.5.2 | Mechanical properties and water absorption capacity

Compression tests were performed to investigate the effect of different homogenization techniques on the mechanical properties of scaffolds in terms of compressive strength and modulus (Figure 11). Compression moduli of chitosan scaffolds pretreated with an ultrasonic

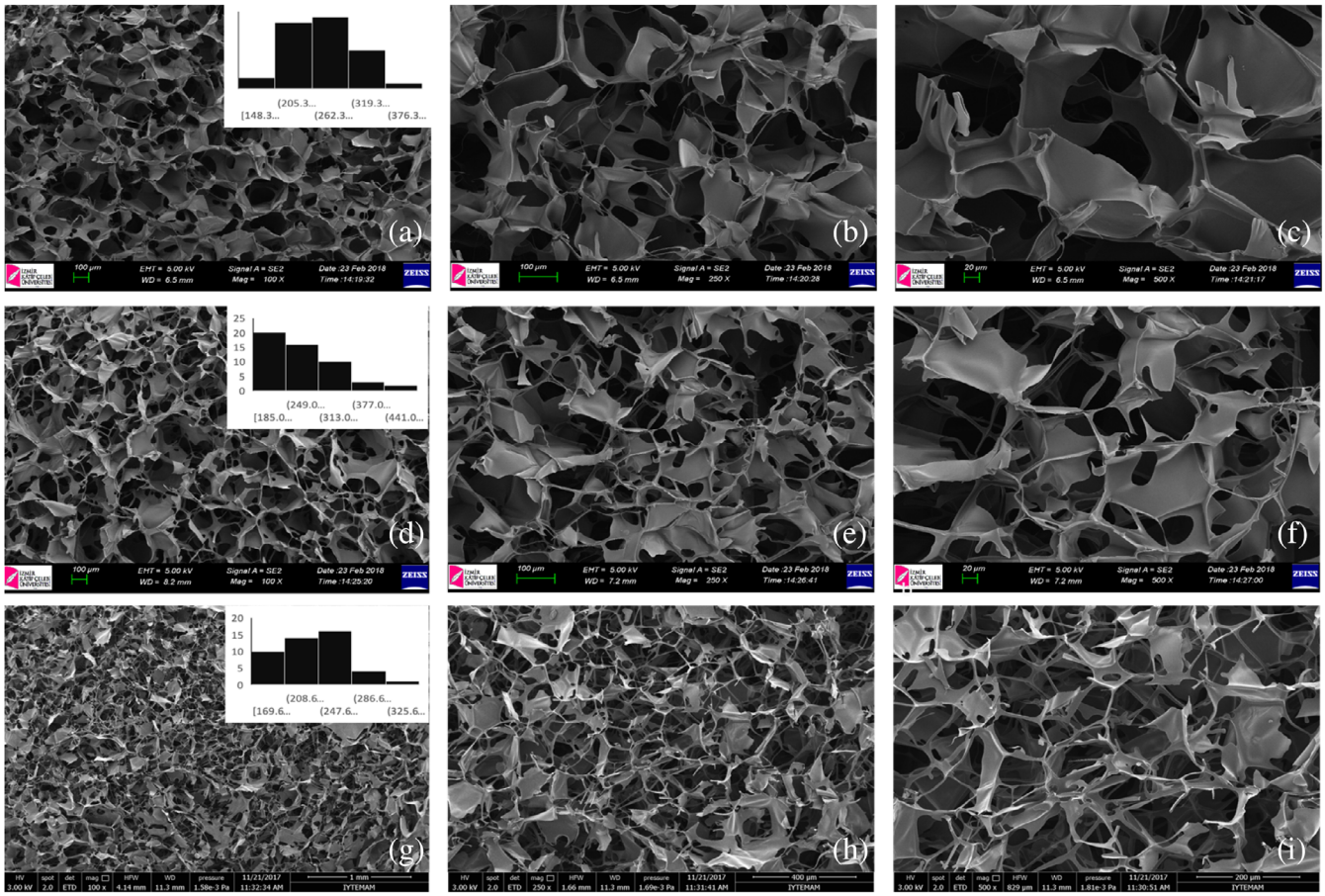

FIGURE 7 SEM images of CS/POSS nanocomposite scaffolds treated with ultrasonic bath (a, b, c); sonicator-15 amp (d, e, f); sonicator-35 amp (g, h, i) in magnification of 100×, 250×, and 500× [Color figure can be viewed at wileyonlinelibrary.com]

bath (661 Pa) were found to be similar to untreated scaffolds (708 Pa). However, sonication pretreatment with both 15 and 35 Amp affected the mechanical properties of the scaffolds negatively. Results supported the morphological observations as the decrease in the compression modulus of groups treated with the sonication (183–466 Pa) could be explained by the asymmetrically distributed microstructure observed in SEM images. On the other hand, compression moduli of CS scaffolds were not affected significantly with microfluidizer pretreatment at 5000 psi pressure (724–755 Pa), then lowered with the increase in pressure from 5000 to 10,000 psi. However, enhanced compression modulus values were observed for both pressure conditions with an increase in the pass number due to the enhanced homogeneity of the microstructures. Compression results of CS/POSS nanocomposites showed that the reinforcement effect of the POSS nanoparticle dispersion in the polymer matrix was observed for all groups. In detail, the highest compression modulus was observed for the group homogenized with the ultrasonic bath (862 Pa), whereas sonication had a lowering effect for this group (200–442 Pa). This effect could be attributed to the low viscosity of the sonicated groups, which leads to irregular pore distributions in the structure. Homogenous and interconnected microstructures obtained with microfluidizer homogenization caused an increment in mechanical characteristics. When the effect of the microfluidizer homogenization was assessed, it was observed that the increase in the pass number from 3 to 5 at constant pressure (5000 psi) improved the mechanical properties (645–846 Pa). This enhancement in mechanical properties can be related to the microstructure of scaffolds depicted in SEM micrographs showing larger and more homogenous pore wall surfaces at 5000 psi compared to other homogenization groups. As observed for pure chitosan scaffolds, a further increase in the pressure to 10,000 psi affected the mechanical properties of the nanocomposite scaffolds negatively due to decreasing viscosity (220–632 Pa).

Biomaterials should absorb the body fluid to allow protein adsorption at the material surface. This initial protein adsorption further ensures cellular attachment and proliferation on the scaffold surface. Thus, the water absorption capacities of scaffolds were determined with

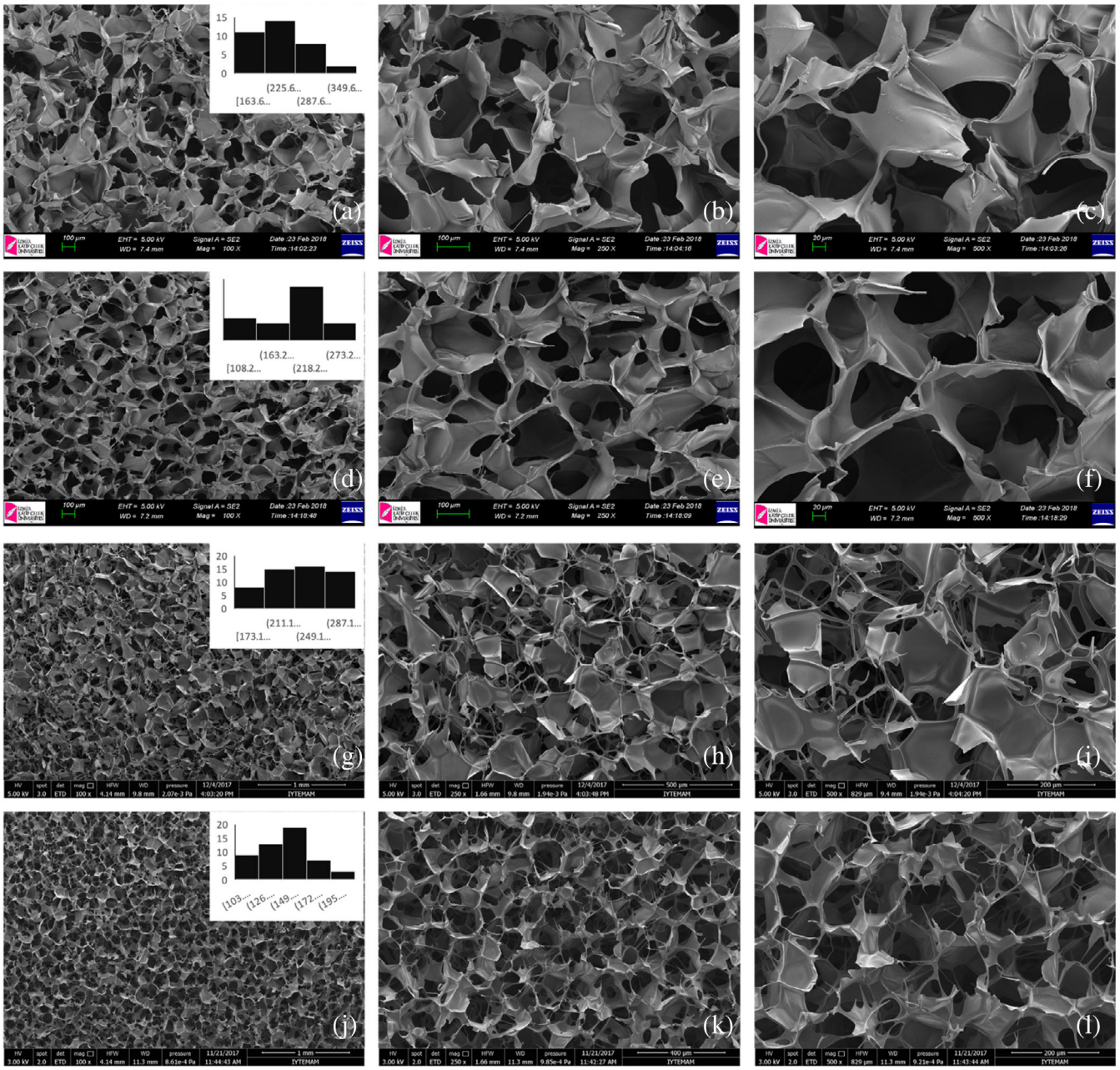

FIGURE 8 SEM images of LMW CS/POSS nanocomposite scaffolds treated with microfluidizer homogenization. Microfluidizer parameters are: 5000 psi 3 pass (a, b, c); 5000 psi 5 pass (d, e, f); 10,000 psi 3 pass (g, h, i); 10,000 psi 5 pass (j, k, l) in magnification of 100×, 250×, and 5000× [Color figure can be viewed at wileyonlinelibrary.com]

the swelling test. The swelling degree of the scaffolds was found in a range of 30–46 (Figure 12). Results indicated that the swelling ratio of CS scaffolds homogenized with ultrasonic bath and sonication at 15 Amp showed a similar trend due to their similar microstructure as shown in SEM images. It was observed that the water absorption capacity was increased with the POSS nanofiller dispersion due to its hydrophilic structure.[55] Additionally, with an increase in pressure and pass number from 5000 to 10,000 psi, scaffolds showed thinner pore walls and higher open porosity, resulting in enhanced water absorption capacity. A significant change in the swelling degree was not observed within different incubation periods, which shows that the absorbed liquid in the nanocomposite matrix was not lost within the first 48 h.

3.5.3 | Thermal degradation

The thermal stability and decomposition behavior of LMW CS and LMW CS/POSS composites were analyzed with thermogravimetric analysis (TGA) (Figure 13).

TABLE 4 Average pore size and porosity % values of LMW CS and LMW CS/POSS scaffolds with different MF operation conditions

	Homogenization parameters	Average lateral pore size (μm)	Open porosity (%)
CS	Non homogenized	213 ± 44	77 ± 0.5
	Ultrasonic bath	199 ± 52	74 ± 12
	Sonicator (15 Amp)	211 ± 55	74 ± 12
	Sonicator (35 Amp)	240 ± 52	83 ± 5
	5000 psi 3 passes	235 ± 72	76 ± 10
	5000 psi 5 passes	221 ± 42	70 ± 5
	10,000 psi 3 passes	277 ± 41	85 ± 1
	10,000 psi 5 passes	281 ± 43	74 ± 4
CS/POSS	Ultrasonic bath	283 ± 52	78 ± 8
	Sonicator (15 Amp)	281 ± 67	75 ± 6
	Sonicator (35 Amp)	239 ± 39	78 ± 2
	5000 psi 3 passes	258 ± 57	77 ± 2
	5000 psi 5 passes	223 ± 55	70 ± 9
	10,000 psi 3 passes	257 ± 40	81 ± 2
	10,000 psi 5 passes	191 ± 33	71 ± 6

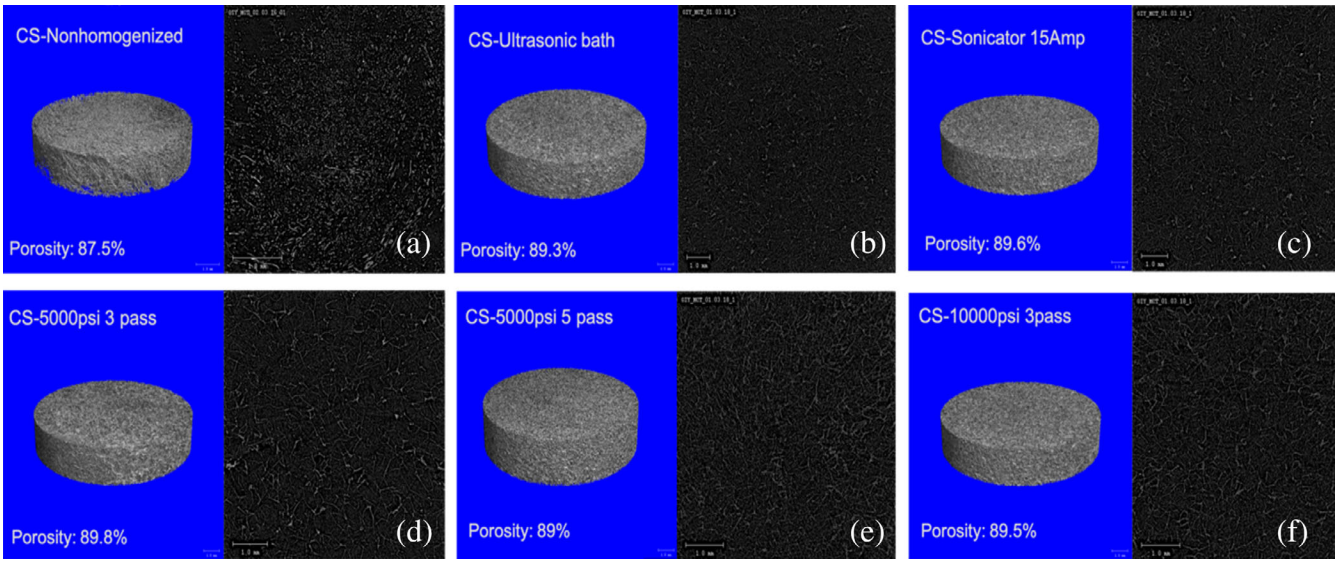

FIGURE 9 Micro-CT images of LMW CS scaffolds with 3D structural view and cross-sectional view: Non homogenized (a); ultrasonic bath (b); Sonicator 15 amp (c), 5000 psi 3 pass (d); 5000 psi 5 pass (e); 10,000 psi 3 pass (f) [Color figure can be viewed at wileyonlinelibrary.com]

Thermal degradation is combination of physical and chemical processes that includes the phase transition, oxidation and decomposition of materials, and it is important for the characterization of the biomaterials for medical applications.[56] Here, it was seen that the microfluidizer homogenization, as well as the conventional methods (ultrasonic bath and sonication) did not cause a remarkable alteration in the thermal stability of the LMW CS matrices. The TGA results indicated that non-homogenized CS and CS scaffolds homogenized with ultrasonic bath showed similar TG trends where MF homogenization showed similar effects with sonication at 15AMP with regard to the transition regimes. Initial weight loss of samples was observed in the range of 30–100°C and this regime was attributed to the dehumidification of the samples. Further, the second decay in the range of 300–400°C regime indicated the thermal degradation as the attributing depolymerization of the polymer matrices. The thermal decomposition in this region is related to the complex dehydration of the saccharide

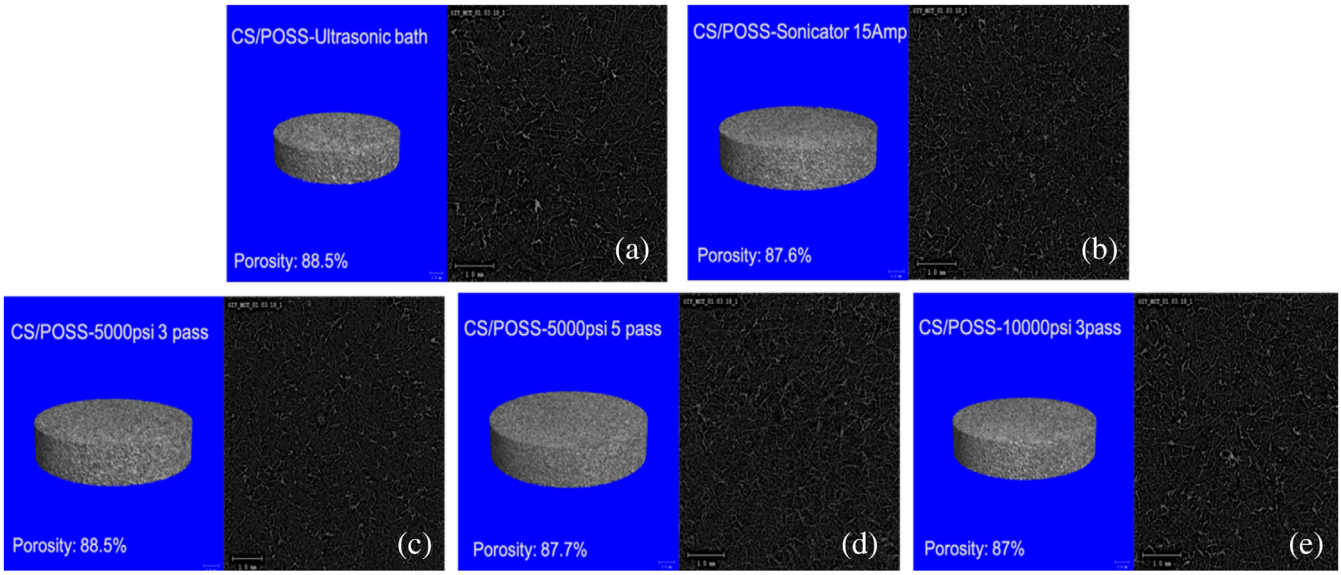

FIGURE 10 Micro-CT images of LMW CS/POSS nanocomposite scaffolds: 3D structural view and cross-sectional view: Ultrasonic bath (a); Sonicator 15 amp (b); 5000 psi 3 pass (c); 5000 psi 5 pass (d); 10,000 psi 3 pass (e) [Color figure can be viewed at wileyonlinelibrary.com]

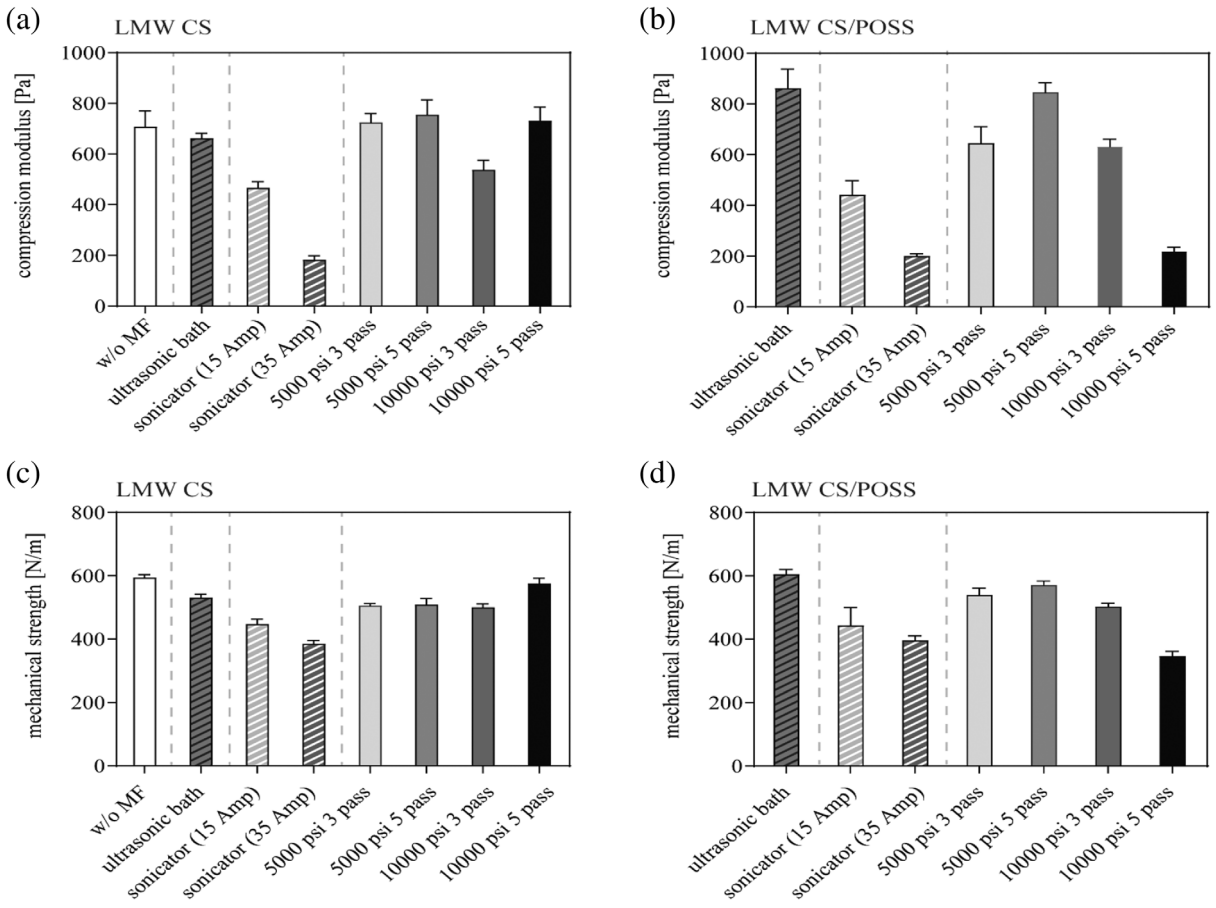

FIGURE 11 Mechanical characterization of the tissue scaffolds. Compression modulus (a, c) and mechanical strength (b, d) of pure chitosan and chitosan/POSS nanocomposite scaffolds, respectively. The mechanical properties of chitosan (a, b) and chitosan/POSS nanocomposite tissue scaffolds (c, d). Error bars denote standard deviation obtained from $n = 5$ independent samples

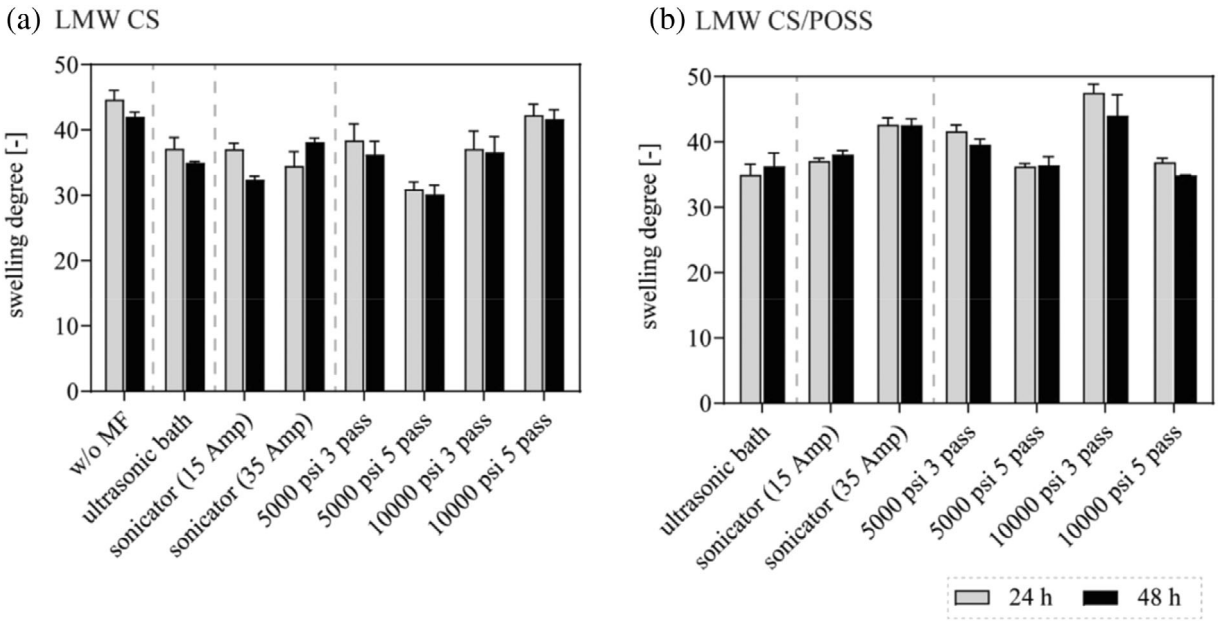

FIGURE 12 The swelling degree of chitosan (a) and chitosan/POSS composite tissue scaffolds (b) after 24 and 48 h of incubation in 1x PBS (pH = 7.4). Error bars denote standard deviation obtained from $n = 5$ independent samples

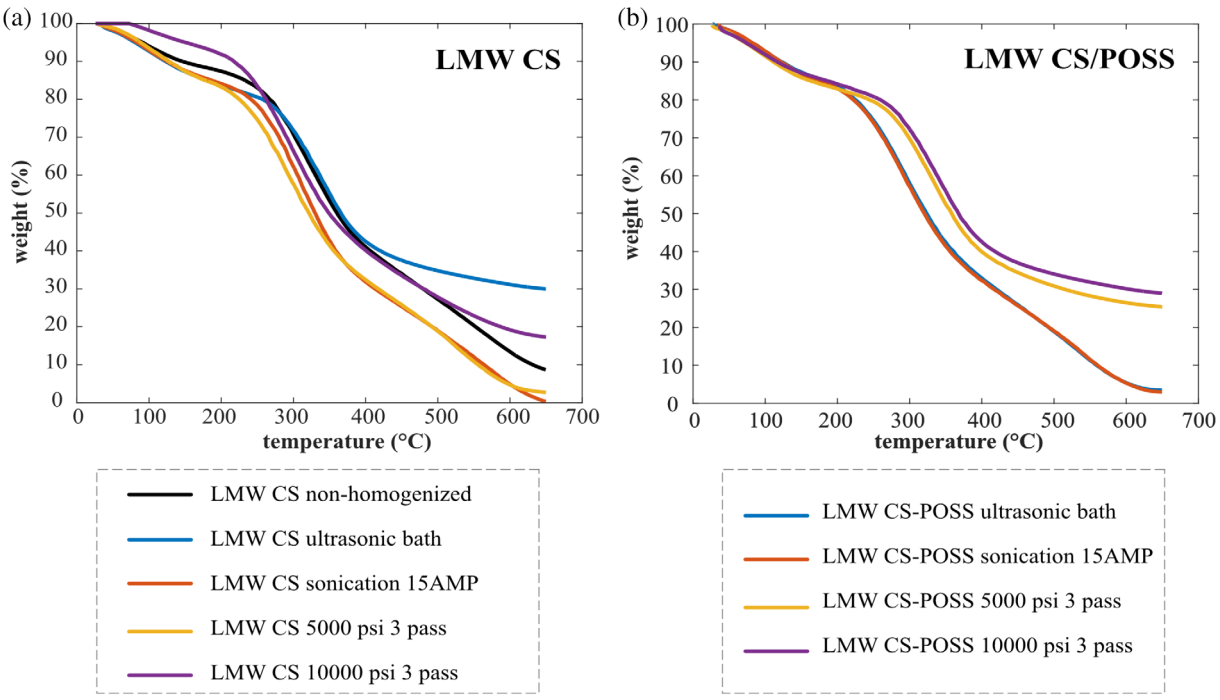

FIGURE 13 TGA thermograms of LMW CS and LMW CS/POSS composites under nitrogen environment [Color figure can be viewed at wileyonlinelibrary.com]

rings and the decomposition of the both acetylated and deacetylated units of the chitosan.[57] However, at 650°C, total weight loss of CS samples altered with different homogenization techniques. TGA of CS/POSS composites showed that conventional techniques (ultrasonic bath and sonication) showed similar degradation trend at 200–300°C. However, microfluidizer homogenization altered the thermal degradation behavior of CS/POSS composites by shifting degradation regime to 300–400°C. Overall weight loss of samples indicated that microfluidizer homogenization decreased the total weight loss of composites at 650°C.

4 | CONCLUSION

This study showed that the microfluidizer homogenization technique could improve the nanoparticle dispersion in high and low molecular chitosan matrices. Besides, microfluidization techniques can be an alternative to conventional homogenization techniques such as ultrasonic homogenization, which causes drastic changes in the viscosity of biopolymer solutions. Results indicated that the microfluidization process altered the solution characteristics at a minimum level compared to the conventional techniques, provided homogenous distribution, and positively affected the fabricated nanocomposites' physical properties. By using this technique, an efficient nanofiller dispersion and a consecutive reinforcement effect were observed in both nano and macroscale chitosan nanocomposites compared to the conventional ultrasonic homogenization methods. The low stability of the chitosan nanospheres was obviated with the MMT reinforcement, which leads to uniform size distribution and high drug encapsulation efficiency.

Furthermore, 3D tissue scaffolds obtained by MF technique (CS/POSS nanocomposites) showed high porosity and interconnected pores, good mechanical properties, and adequate swelling degree due to successful reinforcement in the structure. Thermal stability of CS/POSS composites altered with microfluidizer homogenization compared to conventional homogenization methods. These findings demonstrate that the microfluidizer is a powerful technique to supply improved homogeneity of nanocomposite biomaterials for various biomedical applications. It is a more appropriate method to process biopolymers regarding the property requirements.

AUTHOR CONTRIBUTIONS

Ceren Kimna: Data curation (equal); investigation (equal); methodology (equal); validation (equal); visualization (equal); writing – original draft (equal); writing – review and editing (equal). **Sibel Deger:** Data curation (equal); investigation (equal); methodology (equal); visualization (equal). **Sedef Tamburaci:** Conceptualization (equal); data curation (equal); investigation (equal); methodology (equal); supervision (equal); validation (equal); writing – original draft (equal); writing – review and editing (equal). **Funda Tihminlioglu:** Conceptualization (lead); funding acquisition (lead); investigation (equal); methodology (equal); project administration (lead); resources (lead); supervision (lead); validation (equal); visualization (equal); writing – original draft (equal); writing – review and editing (lead).

ACKNOWLEDGMENTS

The authors acknowledge the Center for Materials Research (IZTECH CMR) of Izmir Institute of Technology, Central Research Laboratories Application and Research Center of Izmir Katip Celebi University for SEM analyses; Central Research Test and Analysis Laboratory Application and Research Center in Ege University for micro-CT analyses. Dr. Gülnihal Yelken for DLS measurements, and Dr. Ozlem Caglar Duvarci for rheology analyses. This study was financially supported by The Scientific and Technological Research Council of Turkey (TUBITAK) under the name of Development of Controlled Antibiotic Releasing Chitosan/Silica Based Composite Scaffolds and Investigation of Their Potential for Hard Tissue Engineering Applications (1001-#116M096).

DATA AVAILABILITY STATEMENT

The data that support the findings of this study are available from the corresponding author upon reasonable request.

ORCID

Funda Tihminlioglu https://orcid.org/0000-0002-3715-8253

REFERENCES

[1] N. Reddy, R. Reddy, Q. Jiang, *Trends Biotechnol.* **2015**, *33*, 362.
[2] S. Pina, J. M. Oliveira, R. L. Reis, *Adv. Mater.* **2015**, *27*, 1143.
[3] W. Zhu, F. Masood, J. O'Brien, L. G. Zhang, *Nanomed.: Nanotechnol., Biol. Med.* **2015**, *11*, 693.
[4] K.-W. Lee, S. Wang, M. J. Yaszemski, L. Lu, *Biomaterials* **2008**, *29*, 2839.
[5] P. N. Christy, S. K. Basha, V. S. Kumari, A. K. H. Bashir, M. Maaza, K. Kaviyarasu, M. V. Arasu, N. A. al-Dhabi, S. Ignacimuthu, *J. Drug Delivery Sci. Technol.* **2020**, *55*, 101452.
[6] S. Tamburaci, C. Kimna, F. Tihminlioglu, *Mater. Sci. Eng., C* **2019**, *100*, 196.
[7] V. Thomas, S. Jagani, K. Johnson, M. V. Jose, D. R. Dean, Y. K. Vohra, E. Nyairo, *J. Nanosci. Nanotechnol.* **2006**, *6*, 487.
[8] M. Rasoulzadeh, H. Namazi, *Carbohydr. Polym.* **2017**, *168*, 320.
[9] S. Y. Raut, A. Gahane, M. B. Joshi, G. Kalthur, S. Mutalik, *J. Drug Delivery Sci. Technol.* **2019**, *51*, 234.
[10] A. Verma, U. Riaz, *J. Drug Delivery Sci. Technol.* **2018**, *48*, 49.
[11] D. R. Paul, L. M. Robeson, *Polymer* **2008**, *49*, 3187.
[12] J. Shojaeiarani, D. Bajwa, G. Holt, *NANO* **2020**, *6*, 41.
[13] T. Panagiotou, J. M. Bernard, S. V. Mesite, in *Nano Science and Technology Institute (NSTI) Conference and Expo Proceedings*. NSTI-Nanotech: Boston, MA **2008**.
[14] J. Chen, R. H. Liang, W. Liu, C. M. Liu, T. Li, Z. C. Tu, J. Wan, *Food Hydrocolloids* **2012**, *28*, 121.
[15] S. M. Jafari, Y. He, B. Bhandari, *Int. J. Food Prop.* **2006**, *9*, 475.
[16] Á. Perdones, I. Escriche, A. Chiralt, M. Vargas, *Food Chem.* **2016**, *197*, 979.
[17] K. Kuhn, R. Cunha, *J. Food Eng.* **2012**, *111*, 449.
[18] X. Song, C. Zhou, F. Fu, Z. Chen, Q. Wu, *Ind. Crops Prod.* **2013**, *43*, 538.
[19] O. K. Ozturk, H. Turasan, *Trends Food Sci. Technol.* **2021**, *116*, 609.

[20] M. S. Alkanawati, F. R. Wurm, H. Thérien-Aubin, K. Landfester, *Macromol. Mater. Eng.* **2018**, *303*, 1700505.
[21] Y. Wei, C. Wang, X. Liu, A. Mackie, L. Zhang, J. Liu, L. Mao, F. Yuan, Y. Gao, *Food Res. Int.* **2020**, *138*, 109817.
[22] M. R. Kasaai, G. Charlet, P. Paquin, J. Arul, *Innovative Food Sci. Emerging Technol.* **2003**, *4*, 403.
[23] Z. Flores, D. San Martín, R. Villalobos-Carvajal, G. Tabilo-Munizaga, F. Osorio, J. Leiva-Vega, *Food Hydrocolloids* **2016**, *61*, 851.
[24] M. Vargas, Á. Perdones, A. Chiralt, M. Cháfer, C. González-Martínez, *Food Hydrocolloids* **2011**, *25*, 1158.
[25] M. Corredig, L. Wicker, *Food Hydrocolloids* **2001**, *15*, 17.
[26] M. R. De Moura et al., *J. Food Eng.* **2011**, *104*, 154.
[27] A. Khan, K. D. Vu, G. Chauve, J. Bouchard, B. Riedl, M. Lacroix, *Cellulose* **2014**, *21*, 3457.
[28] Y. Norzita, T. Norhashidah, and M. Maznah, Determination of viscosity-average molecular weight of chitosan using intrinsic viscosity measurement. **2013**.
[29] J. G. Domszy, G. A. Roberts, *Die Makromol. Chem.* **1985**, *186*, 1671.
[30] A. Kara, S. Tamburaci, F. Tihminlioglu, H. Havitcioglu, *Int. J. Biol. Macromol.* **2019**, *130*, 266.
[31] S. Dan, M. Kalantari, A. Kamyabi, M. Soltani, *Polym. Bull.* **2021**, 1. https://doi.org/10.1007/s00289-021-03903-7
[32] S. Banivaheb, S. Dan, H. Hashemipour, M. Kalantari, *J. Saudi Chem. Soc.* **2021**, *25*, 101283.
[33] Z. Yu, B. Li, J. Chu, P. Zhang, *Carbohydr. Polym.* **2018**, *184*, 214.
[34] F. S. Rezaei, F. Sharifianjazi, A. Esmaeilkhanian, E. Salehi, *Carbohydr. Polym.* **2021**, *273*, 118631.
[35] C. J. Geankoplis, Transport processes and separation process principles: (includes unit operations). Prentice Hall Professional Technical Reference, **2003**.
[36] I. Choi, Y. Chang, S. H. Shin, E. Joo, H. Song, H. Eom, J. Han, *Int. J. Mol. Sci.* **2017**, *18*, 1278.
[37] N. Lagoueyte, P. Paquin, *Food Hydrocolloids* **1998**, *12*, 365.
[38] L. Salvia-Trujillo, M. A. Rojas-Graü, R. Soliva-Fortuny, O. Martín-Belloso, *Food Hydrocolloids* **2013**, *30*, 401.
[39] L. Del Blanco et al., *Colloid Polym. Sci.* **1999**, *277*, 1087.
[40] T. Minagawa, Y. Okamura, Y. Shigemasa, S. Minami, Y. Okamoto, *Carbohydr. Polym.* **2007**, *67*, 640.
[41] E. Tombácz, M. Szekeres, *Appl. Clay Sci.* **2006**, *34*, 105.
[42] K. S. Katti, D. R. Katti, R. Dash, *Biomed. Mater.* **2008**, *3*, 034122.
[43] L. Liu, X. Xu, *J. Therm. Anal. Calorim.* **2016**, *124*, 743.
[44] L. Legnani, D. Iannazzo, A. Pistone, C. Celesti, S. Giofrè, R. Romeo, A. di Pietro, G. Visalli, M. Fresta, P. Bottino, I. Blanco, M. A. Chiacchio, *RSC Adv.* **2020**, *10*, 11325.
[45] E. Tang, M. Huang, L. Y. Lim, *Int. J. Pharm.* **2003**, *265*, 103.
[46] S. Honary, F. Zahir, *Trop. J. Pharm. Res.* **2013**, *12*, 265.
[47] F. Xavier-Jr et al., *J. Drug Delivery Sci. Technol.* **2019**, *53*, 101194.
[48] K. Gupta, F. H. Jabrail, *Carbohydr. Res.* **2006**, *341*, 744.
[49] S. Rodrigues, M. Dionísio, C. R. López, A. Grenha, *J. Funct. Biomater.* **2012**, *3*, 615.
[50] F. Croisier, C. Jérôme, *Eur. Polym. J.* **2013**, *49*, 780.
[51] H.-Y. Cheung, K. T. Lau, T. P. Lu, D. Hui, *Composites, Part B* **2007**, *38*, 291.
[52] F. Baino, S. Fiorilli, C. Vitale-Brovarone, *Acta Biomater.* **2016**, *42*, 18.
[53] V. Karageorgiou, D. Kaplan, *Biomaterials* **2005**, *26*, 5474.
[54] A. R. Costa-Pinto, R. L. Reis, N. M. Neves, *Tissue Eng., Part B* **2011**, *17*, 331.
[55] E. Ayandele, B. Sarkar, P. Alexandridis, *Nanomaterials* **2012**, *2*, 445.
[56] Z. Zhang, G. Liang, X. Wang, *Polym. Bull.* **2007**, *58*, 1013.
[57] S. Mendioroz, M. Belzunce, J. Pajares, *J. Therm. Anal. Calorim.* **1989**, *35*, 2097.

SUPPORTING INFORMATION

Additional supporting information can be found online in the Supporting Information section at the end of this article.

How to cite this article: C. Kimna, S. Deger, S. Tamburaci, F. Tihminlioglu, *J. Appl. Polym. Sci.* **2022**, *139*(40), e52955. https://doi.org/10.1002/app.52955